JOURNAL OF AEROSPACE COMPUTING, INFORMATION, AND COMMUNICATION
Vol. 8, June 2011

Measurement and Modeling of Multiantenna Systems in Small Aircraft

P. R. Sai Ananthanarayanan* , Alyssa Magleby Richards† , and Cynthia Furse‡
University of Utah, Salt Lake City, UT 84112-9206

DOI: 10.2514/1.51492

Multiantenna measurements were performed in three small aircraft (Beech Baron 58-P, Rockwell T-39 Sabreliner, and the Diamond DA-42 Twin Star) and compared to those of six statistical multiantenna channel models, being the Gaussian, Nakagami-*m*, Weibull, hyper-Rayleigh, virtual, and Weichselberger models. The results were also compared to that of a site-specific 3D ray-tracing-based model. The effects of the measurement system, like antenna polarization and radiation pattern, were added to all of the models. It was found that the 3D ray-tracing model provides the most accurate predictions, closely followed by the Nakagami-*m* and Gaussian models. Differences between measured and modeled data were typically less than 1 bit/s/Hz for the three aircraft for the 3D ray-tracing model. For the Nakagami-*m* model, the differences were typically in the range of 0.5–1.5 bits/s/Hz whereas the Gaussian model had differences typically in the range of 1–2 bit/s/Hz. The simpler statistical hyper-Rayleigh model gives differences of the order of 2–3 bit/s/Hz for the Beech Baron 58-P and 3–5 bits/s/Hz for the Rockwell T-39 Sabreliner. The virtual and Weichselberger models were in the range of 2–4 bits/s/Hz.

I. Introduction

WIRELESS data transfer in aircraft has been identified as a "transformative" technology for aviation. Present wireless aircraft systems include smoke detection based on photoelectric smoke and temperature sensors, video security, and emergency lighting control and rotary displacement sensors for providing information required for flight control operation [1–3]. The aircraft wireless intercommunications system involves the use of ultra-wideband signals for communication in order to free up crew members from the cumbersome cables that connect their headsets to the aircraft [4]. Numerous other sensors for improving safety and reliability [5] have been proposed for aircraft, thus increasing the probable future demand for wireless communication in aircraft. In [6], we used a single transmitter location and worked to optimize selected antenna designs in that environment. The purpose was to determine if additional more advanced antenna optimization might yield better system designs in this environment.

Wireless communication in aircraft is challenging because of the multipath reflections caused by the closed metallic structure, signal loss because of tightly packed bodies, and broad band noise channel from existing avionics, radar, etc. and the need to limit the transmission signal in order to ensure no interference between flight critical

Received 6 July 2010; accepted for publication 14 February 2011.

* Post Doctoral Research Fellow, Electrical and Computer Engineering, and AIAA Student Member, 50 S. Central Campus Dr., Rm. 3280 MEB Salt Lake City, UT 84112-9206, saianantha21@gmail.com.

† Instructor, Electrical and Computer Engineering, University of Alabama, 317 Houser Hall, Tuscaloosa, AL 35487-0286, alyssamrichards@gmail.com, aly.magleby@gmail.com.

‡ Professor, Electrical and Computer Engineering, 50 S. Central Campus Dr., Rm. 3280 MEB Salt Lake City, UT 84112-9206, efurse@ece.utah.edu.

communication and for less critical applications such as nonessential sensors and entertainment. Single antenna channel measurements were reported by Frolik et al. [7–9] in various small and midsize aircraft and helicopter environments. They found the aircraft channel to have a Rayleigh or hyper-Rayleigh (HR) distribution. Matolak and Chandrasekaran [10] performed single antenna channel measurements in midsize aircraft at 5 GHz and found the aircraft channel to have a Weibull or Nakagami-m type distribution. The measurements in [7–10] provide a starting point for our multiantenna investigation. Measurements of both single and multiantenna systems were taken in a Rockwell T-39 Sabreliner (composite body), Diamond DA-42 Twin Star (composite body), and Beech Baron 58-P (metallic body) aircraft. Several transmitter and receiver locations were measured, with 100 measurements performed at each location. These measurements are described in Sec. II (single antenna) and III (multiantenna).

One of the potential methods of increasing the communication capacity in a rich multipath environment such as aircraft is to use a multiantenna communication system. Without additional bandwidth, idealized multiantenna capacity grows linearly with increasing antenna element counts [11,12]. More realistic capacity predictions are lower, limited by correlation in the channel and coupling between the antennas [13,14]. Because the capacity is so dependent on the channel propagation properties, having a proper model for the channel is very important in order to correctly predict multiantenna capacity. Several channel models were used or proposed in the past, and this paper compares those models to the multiantenna capacity measured in metallic and composite-skin small body aircraft.

From the single antenna measurements, the multipath channel statistics that give the channel loss, depth of fade, and Ricean K-factor (a measure of the multipath richness) were obtained. This data was incorporated into various multiantenna statistical channel models to predict the capacity expected for a 4×4 multiantenna system. The channel models can generally be divided into two basic groups—the statistical models based on information theory [11] and the site-specific models based on measurement or detailed simulation [13,14]. A detailed channel model was developed by combining the channel model from either a statistical model or the site specific ray-tracing model with the hardware effects including antenna mutual coupling, channel correlation, and receiver mismatch that reduce the multiantenna capacity [13]. Six statistical models (Gaussian, HR, virtual channel model, Weichselberger, Weibull, and Nakagami-m) were compared. The HR model is a statistical model that defines the channel as having two strong waves with diffuse power and is also sometimes called the two-wave with diffuse power (TWDP) model [7]. The Weibull model has been used indoors, outdoors, and in aircraft environments [15,16]. The Nakagami-m distribution has one more free parameter than the Weibull model which allows for increased flexibility. Moreover, it contains both the Rayleigh distribution ($m = 1$) and the uniform distribution on the unit circle ($m \to \infty$) as special (extreme) cases [17]. The virtual channel model provides a similar model but with relaxed constraints on the correlation separability [18]. The Weichselberger model further relaxes these constraints and develops the channel matrix for a correlated channel [18,19]. None of these models are site-specific. They provide a statistical approximation to the channels in the overall aircraft and are described in more detail in Sec. III. Along with these, we also study a 3D site-specific ray-tracing channel model based on models previously used for indoor channel prediction [20,21]. This model is validated by the channel measurements. Once validated, this model could be used to predict site-specific effects in aircraft during the design phase. Section IV briefly describes the detailed signal model for multiantenna systems and the 3D ray-tracing model adapted to the aircraft environment.

Capacity expresses the maximum rate at which information can be transferred reliably in a multiantenna system and is a function of the channel matrix $\mathbf{H}$, which can be directly measured or simulated. Multiantenna channel models described earlier were used to determine $\mathbf{H}$ and therefore the capacity at each of the measurement locations in the aircraft. The goal was to identify the most promising channel models and to determine if there is a common model that is best for the three aircraft. This comparison is described in Sec. V.

II. Single Input Single Output Channel in Aircraft

Single input single output (SISO) channel analysis provides information about the nature of multipath in the aircraft. The depth of fade and the Ricean K-factor were measured at various locations in the Beech Baron, Sabreliner, and Twin Star aircraft in order to quantify the multipath channels. Measurements were performed at 915 MHz using an Agilent E4438C signal generator as the transmitter and Agilent E4407B spectrum analyzer as the receiver. The frequency was chosen to match with the frequency of the multiantenna test bed that was used for multiantenna measurements described in Sec. III. Two 915 MHz monopole antennas were attached to aluminum ground planes. For each location of interest, the received power was measured on a 20×20 grid of points 0.6 inches apart. The

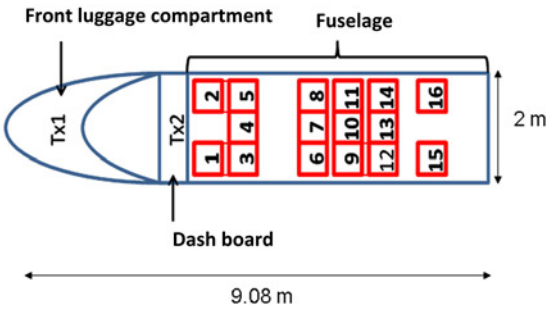

Fig. 1 Transmit and receive locations in the Beech Baron BE 58-P. Test locations for the receiver array are marked with numbered boxes. Tx1 was placed in the luggage compartment in the front nose. Tx2 was placed on the front dashboard. Rx1–Rx16 were located inside the fuselage.

Ricean K-factor was computed from the cumulative distribution function of the measured received power. The depth of fade was obtained from the difference between the maximum and minimum received power in the 400 measured values.

Figure 1 shows the transmitter and receiver locations for the Beech Baron 58-P. This aircraft is a typical metallic-bodied small commuter aircraft (29.8 feet from nose to tail). Measurements for a single antenna system were taken for two different transmitter locations—in the luggage compartment in the nose (Tx1) and on the front copilot dashboard (Tx2). The receiver was moved through 16 locations inside the fuselage, and at each location 400 measurements were taken with a separation of 0.6 inches between measurements. The K-factor was found to be in the range of 0–10 dB. The depth of fade for these two transmitter locations was in the range of 20–30 dB.

Figure 2 shows the transmit and receive locations for the Rockwell T-39 Sabreliner. This aircraft is another small commuter aircraft (47 feet from nose to tail) with a composite body. Measurements were taken for three different transmitter locations—at the center of the dashboard in the cockpit (Tx1), in the maintenance bay underneath the tail (Tx2), and in a centralized location in the cabin (Tx3). The receiver was moved through 17 locations inside the fuselage for locations Tx1 and Tx2 and through 16 locations for Tx3. The Ricean K-factor was in the range of 0–10 dB for all transmitter and receiver locations, except for transmitter Tx3 locations Rx7 and Rx9 where the Ricean

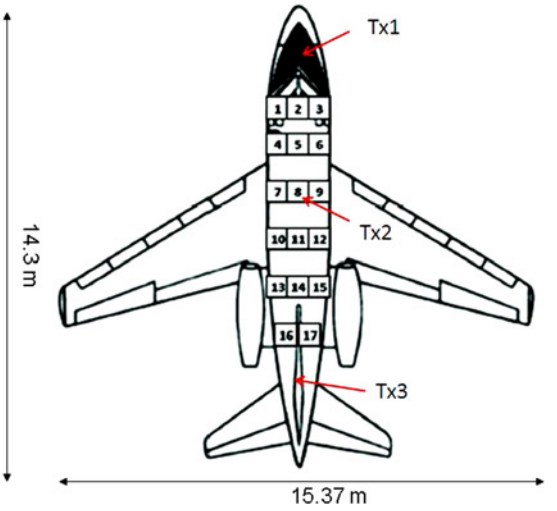

Fig. 2 Transmit and receive locations in the Rockwell T-39 Sabreliner. Tx1 was placed on the dashboard of the cockpit. Tx2 was in a maintenance bay in the tail. Tx3 was located at Rx8 in the center of the fuselage. Rx1–Rx17 were located inside the fuselage.

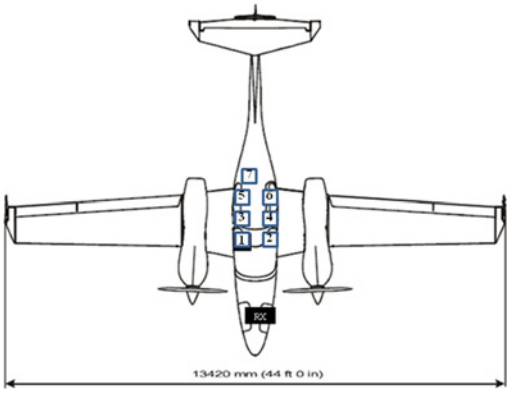

Fig. 3 Transmit and receive locations in the Diamond DA-42 Twin Star. Tx1 was placed in the front luggage compartment. Rx1–Rx7 were located inside the fuselage.

K-factor was 13 and 15 dB, respectively, which was due to the metallic structure present in front of these locations. Figure 3 shows the transmit and receive locations for the Diamond DA-42 Twin Star. This is a small-size commuter aircraft (27 feet from nose to tail) with a composite body. Measurements were taken for a single transmitter location Tx located in the front luggage compartment and for seven receive locations distributed inside the fuselage. The Ricean K-factor was in the range of 0–10 dB.

The maximum depth of fade for all the aircraft was in the range of 20–30 dB. The K-factors obtained in this section will be used for the statistical modeling of the multiantenna systems in Sec. IV.

III. Multiantenna Channel Measurements in Aircraft

For the multiantenna measurement four antennas were used at the transmitter and each of the receiver locations. Multiantenna measurements were performed on three aircraft using the University of Utah multiantenna test bed [22]. The test bed is a software-defined radio platform based on the GNU-Radio toolkit. Shown in Fig. 4, the equipment is capable of supporting a 4×4 multiantenna array at a center frequency of 915 MHz with a sampling rate of 800 kHz. The antenna elements were quarter-wavelength (8.2 cm) monopoles mounted vertically on a 38.1×45.72 cm ground plane, separated by a distance of one-quarter wavelength (8.2 cm). The average power radiated by each antenna was fixed at approximately 5 mW, thus radiating roughly 20 mW from the entire four-element array.

The transmitted data packets were designed for a four-quadrature amplitude modulation scheme using differential encoding with 50 kbps of data per antenna. Each packet began with a simple single antenna preamble of 4000 pseudorandom (PN) data bits for phase and timing synchronization by the receiver. The packet then transmitted a multiantenna sequence of 4×4000 PN bits to be used as a training sequence for channel estimation. The packet terminated with a small multiantenna payload of text data to verify proper packet detection in postprocessing.

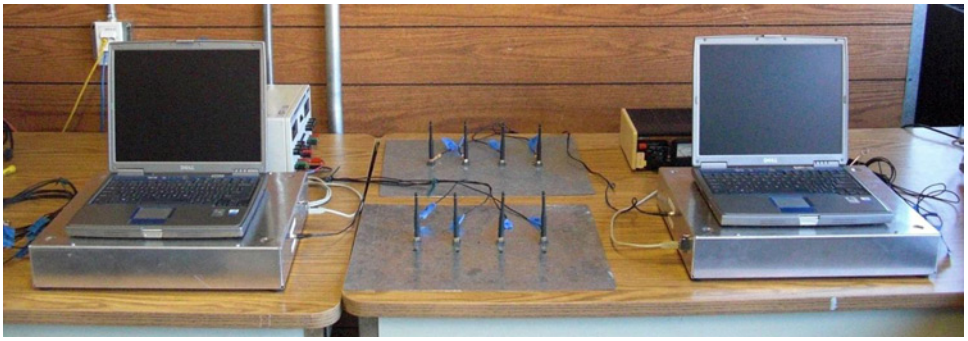

Fig. 4 The University of Utah multiantenna test bed.

Packets were received at a complex baseband with a matched filter. Timing recovery was accomplished using the early–late gate method. Phase was recovered using data-assisted phase rotation. Timing and phase corrections were interpolated to the multiantenna portion after synchronizing to the single antenna packet header. Power normalization was specified by fixing the noise power to unit variance. The channel matrix was estimated using the pseudo-inverse of the training sequence using direct channel-matrix inversion to recover the payload.

Channel measurements were taken for the three aircraft. In the Beech Baron BE 58-P, the measurements were taken for the two transmitter locations shown in Fig. 1. Measurements were also taken in a Rockwell T-39 Sabreliner for the three transmitter locations and the receiver locations shown in Fig. 2. For transmitter location Tx2, the receivers were placed at locations 6, 7, and 10–17, whereas for transmitter location Tx3 the measurements were obtained at locations 1–3, and 10–15. Measurements were taken in a Diamond DA-42 Twin Star for a single transmitter location at the front luggage compartment and for seven receiver locations as shown in Fig. 3.

After placing the receive array at its specified location, a training packet of data was broadcast by the transmit array, thereby providing a direct measurement of the channel matrix for that given transmitter/receiver pair. The receive array was then moved to the next location, and another packet was transmitted. This cycle was repeated until the survey was complete. As long as the environment within the cabin was unchanged over the measurement cycle, all channel matrices may be treated as if they were obtained simultaneously. A fortunate aspect of channel capacity measurements is that one need not physically implement a given algorithm in order to calculate its potential capacity. In fact, the only requisite measurement is a set of **H**-matrices for the various test locations. The channel matrix is computed from a packet of data by defining a complex M $\times$ W matrix **T**, where M is the number of transmit antennas, called the training sequence, and writing it as a series of column vectors with the form

$$\mathbf{T} = [|\mathbf{t}(1)| \quad |\mathbf{t}(2)| \cdots |\mathbf{t}(\mathrm{W})|] \tag{1}$$

In other words, each column vector $\mathbf{t}(w)$ represents an M $\times$ 1 vector of complex data symbols being broadcast by the transmitter. The N $\times$ W matrix of sampled symbols at the receiver may therefore be written as

$$\mathbf{Y} = \mathbf{HT} + \mathbf{N}_{\text{noise}} \tag{2}$$

where $\mathbf{N}_{\text{noise}}$ is simply an N $\times$ W matrix of sampled noise, where N is the number of receive antennas. Because **T** is a known sequence of data, it can be used to estimate the channel matrix as

$$\tilde{\mathbf{H}} = \mathbf{YT}^{+} = \mathbf{H} + \mathbf{N}_{\text{noise}}\mathbf{T}^{+} \tag{3}$$

where $\mathbf{T}^{+}$ denotes the Moore–Penrose pseudo-inverse of **T**, and is given by

$$\mathbf{T}^{+} = (\mathbf{T}^{H}\mathbf{T})^{-1}\mathbf{T}^{H} \tag{4}$$

As long as the signal-to-noise ratio (SNR) at the receiver is relatively large, the effects of the noise term $\mathbf{N}_{\text{noise}}$ are negligible, and $\tilde{\mathbf{H}}$ transforms to **H**. The effects of noise may be further reduced by choosing a relatively large value for W. This is because the quantity $\mathbf{N}_{\text{noise}}\mathbf{T}^{+}$ behaves much like a correlation between the training sequence and the noise. Thus, in the limit as $W \to \infty$, we have $\mathbf{N}_{\text{noise}}\mathbf{T}^{+} \to 0$ for uncorrelated noise. So as long as the channel itself remains stationary over the duration of the training sequence, W may be chosen as any arbitrarily large value. For the data presented in this paper, all channel matrices were estimated using a training sequence of PN data with length $W = 4000$.

IV. Multiantenna Channel Models in Aircraft

This section describes the statistical and 3D ray-tracing models used to estimate the aircraft multipath channel. The statistical models are the Gaussian, HR, Weibull, Nakagami-m, virtual, and Weichselberger models. Each of these models (and the 3D ray-tracing model) are combined with the hardware effects of (among others) antenna mismatch and polarization loss to give a detailed signal model that describes the effects of the antennas in complex channels. The multiantenna capacity predicted by each of these models is compared with the measured capacities at specific locations in the three aircraft to determine which channel model best fits these aircraft.

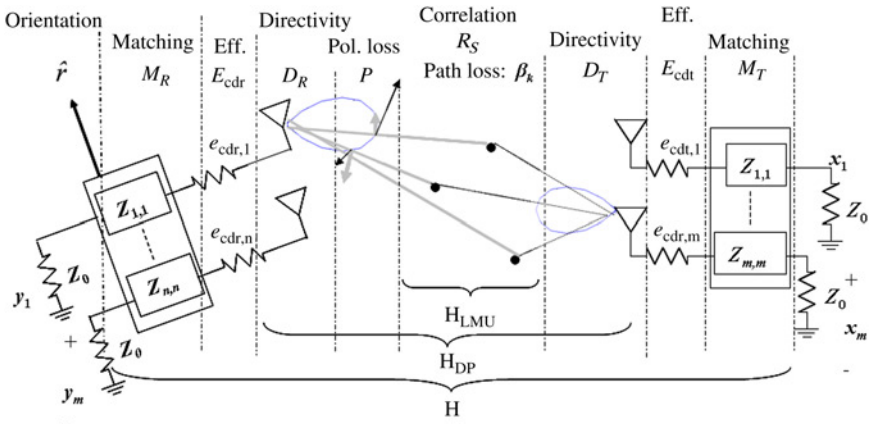

Fig. 5 A general multiantenna setup used to derive the detailed signal model. From [13].

A. Detailed Signal Model

Figure 5 shows the multiantenna system that will be used for deriving the detailed signal model [13]. The model relates transmit input voltages $[x_1 \ldots x_M]$ to receive voltages $[y_1 \ldots y_N]$ as a function of channel and system design parameters. $\mathbf{M}_R$ is the N $\times$ N impedance matrix describing the receive antenna array, and $\mathbf{E}_{\text{cdr}}$ is the diagonal matrix containing the radiation (conduction and dielectric) efficiencies of the Nreceive antennas. $\mathbf{D}_R$ and $\mathbf{P}$ are diagonal matrices of distributed directivities and system polarization alignments, respectively, and $\mathbf{R}_s$ is the spatial correlation of the signals impinging on the receiver—traditionally including the effects expressed in $\mathbf{D}_R$ and $\mathbf{P}$, but broken out separately in our model. Corresponding matrices for the transmit array are denoted by a subscript T or t. Grouping designators are also included for later reference: $\mathbf{H}_{\text{LMU}}$ represents a lossless, matched, uncoupled channel matrix, $\mathbf{H}_{\text{DP}}$ adds directivity and polarization alignment effects, and $\mathbf{H}$ represents a complete system channel matrix:

$$\mathbf{H} = \underbrace{Z_0^{1/2} \underbrace{\mathbf{S}_{21}(\mathbf{I}-\mathbf{S}_{\text{RR}}\mathbf{S}_{11})^{-1}}_{\text{matching}} \left(\mathbf{I}+\frac{\mathbf{Z}_{\text{RR}}}{Z_0}\right)^{-1}}_{M_R} \underbrace{\mathbf{E}_{\text{cdr}}}_{\substack{\text{rad}\\ \text{eff}}} \underbrace{\mathbf{S}_{\text{RT}}}_{H_{\text{DP}}} \underbrace{\mathbf{E}_{\text{cdt}}}_{\substack{\text{rad}\\ \text{eff}}} \underbrace{(\mathbf{I}-\mathbf{S}_{\text{TT}})}_{\text{matching}} \quad (5)$$

$$\mathbf{S}_{\text{RT}} = \sum_{i=1}^{M}\sum_{j=1}^{N}\left[\frac{1}{Z_0}\sum_{k=1}^{N_p} E_i^R(\theta,\phi)\beta_k E_j^T(\theta,\phi)\right] \quad (6)$$

where Z_0 is the characteristic impedance, $\boldsymbol{S}_{TT}$ and $\boldsymbol{S}_{RR}$ are the scattering parameters of the unloaded transmit and receive arrays, respectively; $\boldsymbol{S}_{\text{RT}}$ is the channel scattering matrix; and $\boldsymbol{S}_{11}$ and $\boldsymbol{S}_{21}$ represent a matching circuit and transmission circuit, respectively, for a selected matching approach. The influence of a channel on the channel-system capacity is expressed as a summation of N_p plane waves where the kth plane wave has a complex gain (path loss and phase shifts) of β_k. The $\boldsymbol{S}$ and the $\boldsymbol{Z}$ parameters in Eq. (5) were obtained by simulating the antennas along with the ground plane using the computer simulation technology electromagnetic solver that uses the full wave finite integration technique.

The Weibull distribution has been widely used for modeling the fading envelope in wireless communication. Single antenna measurements [10] show that the Weibull model can accurately estimate the path loss in an aircraft channel at 5 GHz. The Weibull model describes the path loss as

$$\beta_k = R_k^{\alpha/2}\exp(j\Theta_k) \quad (7)$$

where R_k is the Weibull envelope amplitude, Θ_i is the phase, which is uniformly distributed over $[0, 2\pi)$, and α_k is the Weibull fading parameter. The probability density function (pdf) of the Weibull envelope can be written as

$$p_{R_k}(r) = \frac{\alpha_k}{\Omega_k} r^{\alpha_k - 1} \exp\left(-\frac{r^{\alpha_{ki}}}{\Omega_k}\right) \tag{8}$$

where α_k is the Weibull fading parameter and Ω_k is the average fading power. As α_k increases, the fading severity decreases. When $\alpha_k = 2$, this model reduces to the Rayleigh channel model. Weibull channels with various values of α_k and Ω_k were simulated, and the results in Sec. V show that the best capacity estimates are obtained for an $\alpha_k = 1.5$ and $\Omega_k = 1$.

The Nakagami-m distribution provides one more free parameter in the model than the Gaussian and Weibull models, thus providing more flexibility and a better match to most fading channels [17]. The Rayleigh and uniform distribution on the unit circle are special cases of the Nakagami-m model with $m = 1$ and $m = \infty$, respectively. The path loss is again modeled as

$$\beta_k = R_k \exp(j\Theta_k) \tag{9}$$

where R_k has a pdf distribution given by

$$p_R(r) = \frac{2m^m r^{2m-1}}{\Omega_m \Gamma(m)} \exp\left(-\frac{mr^2}{\Omega}\right) \tag{10}$$

where m is the shape parameter and Γ is the spread parameter. The Nakagami model with various values of m were simulated, and the results in Sec. V show that the best capacity estimates are obtained for an $m = 1.4$.

Intra-aircraft and other vehicular channels have been modeled as HR channels. Where the received signal is dominated by two constant amplitude signal components with uniformly distributed angles of arrival over $[0, 2\pi)$, this is also referred to as TWDP, and is described as follows:

$$\sigma = \sqrt{\frac{\beta_1^2 + \beta_2^2}{2K}} \tag{11}$$

where σ is the diffuse parameter and K is the Ricean K-factor. The obtained $\mathbf{S}_{\mathrm{RT}}$ is subsequently substituted in Eq. (5) to obtain the channel matrix $\mathbf{H}$.

B. Virtual Channel Model

The virtual channel model [18] relaxes the correlation separability restrictions of the Kronecker model. The virtual channel matrix can be written as

$$\mathbf{H} = A_{RX}(\mathbf{\Omega}_{\mathrm{virt}} \Theta \mathbf{H}_{\mathrm{iid}}) A_{TX}^T \tag{12}$$

where A_r and A_t are channel independent discrete Fourier transform (DFT) matrices of size 4×4, and Ω_{virt} is the average power coupling matrix between the different transmitter and receiver paths. However, for a practical number of antenna elements, the approximation of the true eigen bases by the predefined DFT matrices can be rather poor. As a consequence, the matrix elements of $\mathbf{H}_{\mathrm{iid}}$ in Eq. (3) can become significantly correlated when the "virtual channel representation" is applied to measured multiple input multiple output (MIMO) channels.

C. Weichselberger Model

The Weichselberger model relaxes the assumption of the Kroneker model by using a power coupling of transmitter and receiver eigenmodes defined by

$$\mathbf{R}_{TX} = \mathbf{U}_{TX} \Lambda_{TX} \mathbf{U}_{TX}^H \quad \text{and} \quad \mathbf{R}_{RX} = \mathbf{U}_{RX} \Lambda_{RX} \mathbf{U}_{RX}^H \tag{13}$$

The channel correlation matrix is modeled as

$$\mathbf{R} = \sum_{i=1}^{N_R} \sum_{i=1}^{N_t} \omega_{ji} (u_{TX,i} \otimes u_{RX,j})(u_{TX,i} \otimes u_{RX,j})^H \tag{14}$$

where ω_{ji} is the element-wise square root of the coupling matrix. The channel matrix is then defined as [19]

$$\mathbf{H} = \mathbf{U}_{RX}(\mathbf{\Omega}\Theta\mathbf{H}_{\text{iid}})\mathbf{U}_{TX}^{T} \tag{15}$$

where $\mathbf{H}_{iid}$ stands for an independent and ideally distributed channel matrix.

D. 3D Ray-Tracing Model

A site-specific 3D ray-tracing model [21] was also used for analyzing the channels in the three aircraft. The model uses the triangular grid method to determine which rays arrive at the receive antenna. The algorithm uses less than 30% of the CPU time of traditional ray-tracing methods and has been validated in 2D indoor and outdoor multipath environments, and in a 3D environment for reflections in stairwells [20]. The software was adapted to a multiantenna system by running the ray tracer multiple times for different antenna locations rather than just a single antenna at a time. The aircraft were modeled with 20 faceted sides to represent the cylindrical shape of the fuselage. Flat plates were used for the front and back of the fuselage. The floor was assumed to be electrically invisible. Additionally, both lossy and reflective internal obstacles were configured, including, for instance, chairs and reflective walls. The aircraft walls were assumed to be perfect electrical conductors for the Beech Baron and were modeled as composite material with permittivity ($\varepsilon_r = 2.2$) for the Twin Star and the Rockwell Sabreliner. Chairs were modeled as two flat surfaces, each with a loss factor of 0.1 dB connected at one edge. This loss factor was estimated based on measured propagation through chairs. Lossy walls within the cabin were modeled as rectangular surfaces with a loss factor of 2.6 dB, which was found to give the most accurate results when varying the wall loss empirically. The antennas were a minimum of 0.01 m from any wall or floor. The maximum number of projected rays was 320, which were attained when 15 or more bounces were allowed before a ray reached the receiver.

The 3D software computes the path loss, angle of arrival, angle of departure, and the electric fields for each transmit–receive pair. These parameters along with the antenna gains were postprocessed to obtain the 3D channel matrix $\mathbf{H}_{3D}$. This was then combined with the various antenna and matching parameters using Eq. (5) to obtain the channel matrix $\mathbf{H}$ (replacing $\mathbf{S}_{RT}$ by $\mathbf{H}_{3D}$).

The capacity for the multiantenna system can be estimated as

$$C = \log_2 \det\left[\mathbf{I} + \frac{\text{SNR}_r N_r}{\|\mathbf{H}\|^2_{\text{Frobenius}}\mathbf{N}_{\text{noise}}}\mathbf{H}\mathbf{H}^{H}\right] \tag{16}$$

To provide consistency of gain between antennas, all sampled data were normalized to a unit noise variance at each antenna. This was accomplished by isolating an unused portion of the spectrum and applying the matched filter as if there were actual data. The resultant noise variance was then used as the normalization factor for the antenna. Also, the channel matrices were normalized in order to eliminate capacity variations due to path loss. For our data, all channel matrices were specifically fixed to a unit Frobenius norm ($\|\mathbf{H}\| = 1$) for all data. Symbol power was then fixed to the arbitrary value of $P_s = 100$, thereby giving an SNR of 20 dB. The channel models developed in this section will be used for calculating capacity as in Eq. (16) and will be compared with the measurements obtained from the three aircraft in Sec. V.

V. Results

In this section, the capacities obtained using the various statistical channel models and the 3D ray-tracing model are compared to those measured in the three aircraft. The capacity provided for the channel models in this section is averaged over 100 simulations.

A. Rockwell T-39 Sabreliner

Figures 6 (location Tx1), 7 (location Tx2), and 8 (location Tx3) show the difference between the measured capacity and the capacity obtained by using the channel models described in Sec. IV for the Rockwell T-39 Sabreliner. From Fig. 6, we observe that the 3D ray-tracing model using the capacity expression in Eq. (16) is accurate to within 1 bit/s/Hz of the measured capacities. Without the front-end parameters included in Eq. (16) and assuming the channel matrix $\mathbf{H} = \mathbf{H}_{3D}$, the error in capacity was about 2–3 bits/s/Hz for location-specific design. The Nakagami-m ($m = 1.4$) model closely follows the 3D ray-tracing model. The Gaussian and Weibull models provide the next best

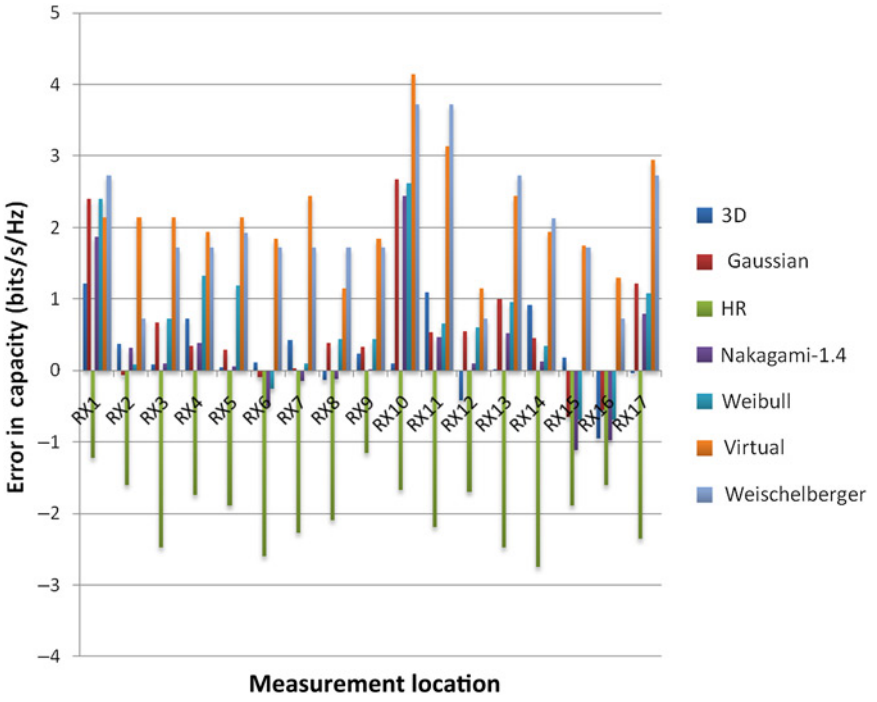

Fig. 6 Difference between the measured and the simulated capacities for the Rockwell T-39 Sabreliner with transmitter Tx1 located at the center of the dashboard in the cockpit.

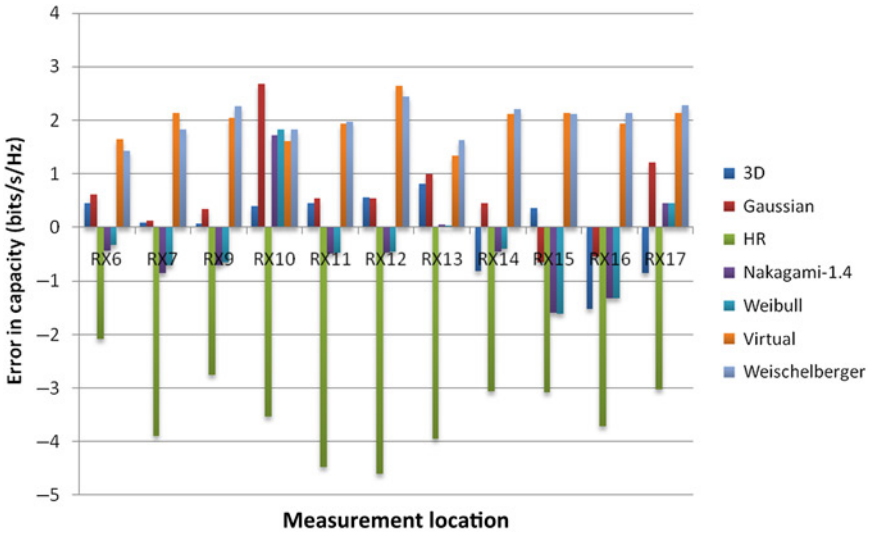

Fig. 7 Difference between the measured and the simulated capacities for the Rockwell T-39 Sabreliner with transmitter Tx2 located in the maintenance bay underneath the tail.

estimates with an error in the range of 1–2 bits/s/Hz, except for a couple of locations where the error is in the range of 2–3 bits/s/Hz. The HR model which inherently assumes less multipath under-predicts the capacity by 2–3 bits/s/Hz. The virtual and the Weichselberger models estimate the capacity in the range of 2–3 bits/s/Hz, except for a couple of locations where error is in the range of 3–4 bits/s/Hz. For transmitters Tx2 and Tx3, the 3D ray-tracing model

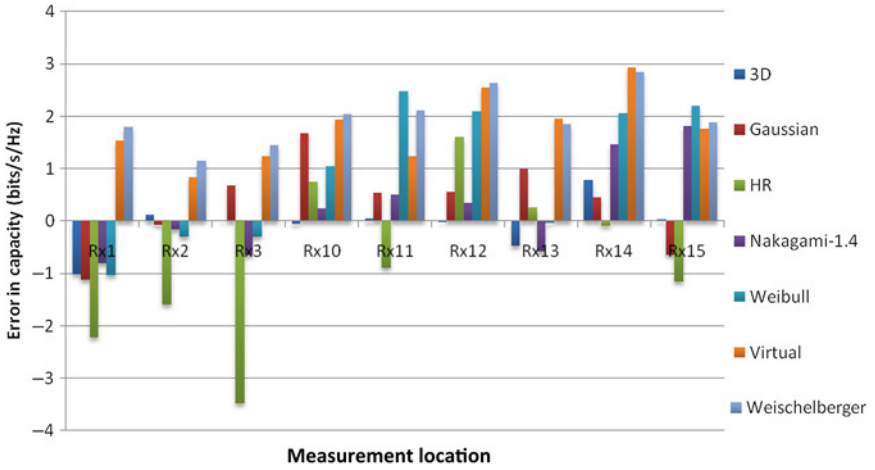

Fig. 8 Difference between the measured and the simulated capacities for the Rockwell T-39 Sabreliner with transmitter Tx3 located in the centralized location within the cabin.

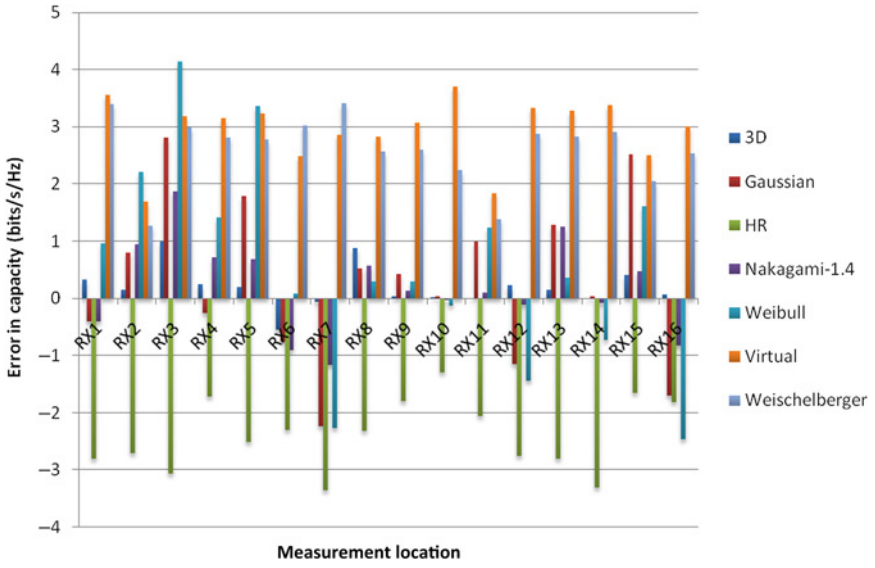

Fig. 9 Difference between the measured and the simulated capacities for the Beech Baron BE 58-P with transmitter Tx1 located in the front luggage compartment.

provides the best estimate to the measured capacity followed by the Nakagami-*m*, Gaussian, and Weibull models, in that order. The virtual and Weichselberger models estimate capacity within 2–3 bits/s/Hz for both cases, whereas the HR model underestimates the capacity by 3–5 bits/s/Hz for Tx2 and 1–3 bits/s/Hz for Tx3.

B. Beech Baron BE 58-P

Figures 9 (location Tx1) and 10 (location Tx2) show the differences between the measured capacity and the capacity obtained by using the channel models for the Beech Baron 58-P aircraft. From the figures, we observe that the 3D ray-tracing model provides the best capacity estimate within 0–1 bit/s/Hz of the measured capacity. The Nakagami-*m* and the Gaussian model follow the 3D ray-tracing model with an estimate of 0–1 bit/s/Hz in most locations, except for a couple of locations where the Gaussian model estimates the capacity in the range of 2–3 bits/s/Hz. The HR model underestimates the capacity by 1.5–3 bits/s/Hz over all locations, whereas the Weibull

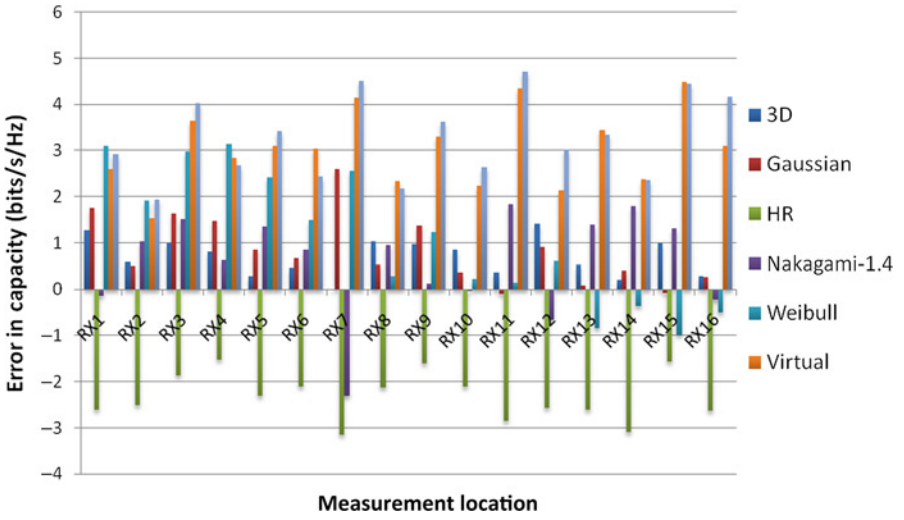

Fig. 10 Difference between the measured and the simulated capacities for the Beech Baron BE 58-P with transmitter Tx2 located at the center of the dashboard in the cockpit.

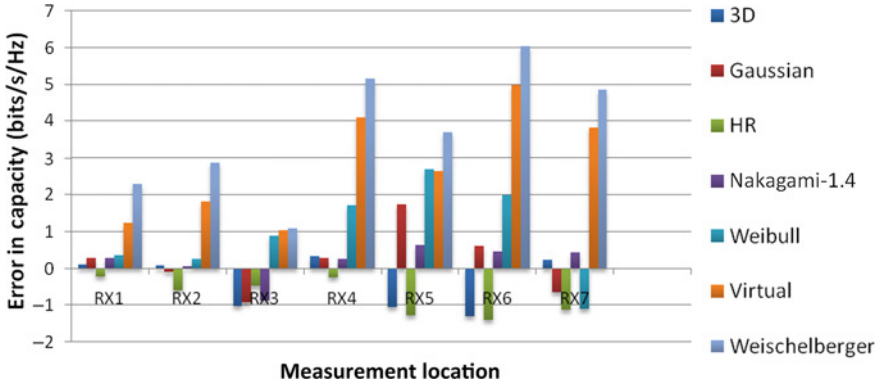

Fig. 11 Difference between the measured and the simulated capacities for the Diamond DA-42 Twin Star with transmitter Tx1 located in the front luggage compartment.

channel overestimates the capacity in the range of 1–2.5 bits/s/Hz. The virtual and Weichselberger channel models overestimate the capacity by 2.5–4 bits/s/Hz.

C. Diamond DA-42 Twin Star

Figure 11 shows the difference between the measured capacity and the capacity obtained by using the channel models for the Diamond DA-42 Twin Star aircraft for transmitter Tx1. From the figure, we observe that the 3D ray-tracing model provides a capacity within 0.5 bit/s/Hz of the measured capacity followed by the Nakagami-*m*, Gaussian, HR, and Weibull channel models in that order. These models estimate the capacity within 0.5–1.5 bits/s/Hz. The virtual and Weichselberger channel models have an error of 1–3 bits/s/Hz for locations Rx1–Rx3 and an error of 3–6 bits/s/Hz for locations Rx4–Rx7. For the composite Diamond DA-42 Twin Star, the HR model provides better capacity approximation to the measured capacity.

Overall, the site-specific 3D ray-tracing model provides the best estimate to the measured capacity in the three aircraft ($\leqslant$0.5 bit/s/Hz) followed by the Nakagami-*m* (0.5–1.5 bits/s/Hz), Gaussian (1–2.5 bits/s/Hz), and Weibull (1–3 bits/s/Hz) models. It is observed that the HR channel underestimates the capacity by an average of 2–4 bits/s/Hz

for the Rockwell T-39 Sabreliner and the Beech Baron 58-P and a deviation of 0.5–1.5 bits/s/Hz for the Diamond DA-42 Twin Star.

VI. Conclusion

This paper analyzes both single and multiantenna communication channels in small aircraft. From the depth of fade and the Ricean K-factor, we observe that the three aircraft have moderate multipath channels. By comparing the measurements with the statistical and 3D ray-tracing based models, we observe that the 3D ray-tracing model provides an accurate estimate to the measured capacity for the three aircraft (error within 0.5 bits/s/Hz). The Nakagami-m model, which has improved flexibility over the simple Gaussian model, follows the 3D ray-tracing model with an average error of 0.5–1.5 bits/s/Hz. The Gaussian and Weibull models estimate the capacity within 1–3 bits/s/Hz to the measured capacity. The HR model inherently assumes less multipath and underestimates the capacity by 3–5 bits/s/Hz. The virtual and Weichselberger models overestimate the capacity by 2.5–4 bits/s/Hz. The 3D ray-tracing model needs information about the exact dimension of the aircraft along with the position of, for instance, chairs, tables, and cabinets to provide an accurate estimate of the system capacity. On the other hand, the statistical models just need the information about the location of sensors along with the Ricean K-factor and multipath. Without the accurate knowledge of the multipath, the statistical models can provide a capacity map with lower and upper bounds which will help the aircraft manufacturers to correctly estimate their system performance.

References

[1] St. John, E., "Operational Issues Wireless Overview," *Presented at the World Airline Entertainment Association Single Focus Workshop (WAEA SFW)*, Washington, D.C., 19–20 Nov. 2002.

[2] Cheng, P., Linnarsson, F., and Oelmann, B., "Joint Angular Sensor Based on Distributed Biaxial MEMS Accelerometers," *Proceedings of the 33rd Annual Conference of the IEEE Industrial Electronics Society, IECON 2007*, 5–8 Nov. 2007, pp. 2242–2247.

[3] Yoo, A., Sul, S., Lee, D., and Seung, C., "Novel Speed and Rotor Position Estimation Strategy Using a Dual Observer for Low Resolution Position Sensors," *IEEE Transactions on Power Electronics*, Vol. 24, No. 12, 2009, pp. 2897–2906.

[4] Ameti, A., Fontana, R., Knight, E., and Richley, E., "Ultra wideband Technology for Aircraft Wireless Intercommunications Systems (AWICS) design," *IEEE Aerospace and Electronic Systems Magazine*, Vol. 19, No. 7, 2004, pp. 14–18.

[5] Furse, C., Smith, P., Lo, C., Chung, Y., Pendayala, P., and Nagoti, K., "Spread Spectrum Sensors for Critical Fault Location on Live Wire Networks," *Structural Control and Health Monitoring*, Vol. 12, No. 3–4, 2005, pp. 257–267.

[6] Sai Ananthanarayanan, P. R., Richards, A. M., and Furse, C., "Wireless and Surface Wave Communication for Aircraft Sensor Networks," *Proceedings of the Aircraft, Airworthiness and Sustainment Conference*, 10–13 May 2010.

[7] Frolik, J., "A Case for Considering Hyper-Rayleigh Fading Channels," *IEEE Transactions on Wireless Communications*, Vol. 6, No. 4, 2007, pp. 1235–1239.

[8] Fitzhugh, C., Frolik, J., Ketcham, R., Covell, J., and Meyer, T., "2.4 GHz Multipath Environments in Airframes," *Proceedings of the IEEE Conference on Wireless and Microwave Technology (WAMICON 2005)*, 6–7 April 2005.

[9] Ketcham, R., Frolik, J., and Covell, J., "Propagation Measurement and Statistical Modeling for Wireless Sensor Systems Aboard Helicopters," *IEEE Transactions on Aerospace and Electronic Systems*, Vol. 44, No. 4, 2008, pp. 1609–1615.

[10] Matolak, D., and Chandrasekaran, A., "Aircraft Intra-vehicular Channel Characterization in the 5 GHz Band," *Proceedings of the Integrated Communications, Navigation and Surveillance Conference*, *ICNS 2008*, 16–21 March 2008, pp. 1–6.

[11] Foschini, G., and Gans, M., "On Limits of Wireless Communications in a Fading Environment When using Multiple Antennas," *Wireless Personal Communications*, Vol. 6, No. 3, 1998, pp. 311–335.

[12] Telatar, I., "Capacity of Multi-antenna Gaussian Channels," *European Transactions on Telecommunications*, Vol. 10, No. 6, 1999, pp. 585–596.

[13] Landon, D., "Polarization Misalignment and the Design and Analysis of Compact Multiple Input Multiple Output Arrays," Ph.D. Dissertation, Univ. Utah, 2007.

[14] Wallace, J., and Jensen, M., "Mutual Coupling in MIMO Wireless Systems: A Rigorous Network Theory Analysis," *IEEE Transactions on Wireless Communications*, Vol. 3, No. 4, 2004, pp. 1317–1325.

[15] Lupupa, M., and Dlodlo, M. E., "Performance of MIMO System in Weibull Fading Channel-Channel Capacity Analysis," *IEEE EUROCON*, 18–23 May 2009, pp. 1735–1740.

[16] Abualhaol, I. Y., and Matalgah, M. M., "Capacity Analysis of MIMO System over Ideally Independent Distributed Weibull Fading Channels," *Proceedings of the IEEE International Conference on Communication, ICC 2007*, 24–28 June 2007, pp. 5003–5008.

[17] Fraidenraich, G., Leveque, O., and Cioffi, J., "On the MIMO Channel Capacity for the Nakagami-m Channel," *IEEE Transactions on Information Theory*, Vol. 54, No. 8, 2008, pp. 3752–3757.

[18] Oestges, C., and Clerckx, B., *MIMO Wireless Communications: From Real-World Propagation to Space-Time Code Design*, Academic Press, New York, 2007.

[19] Weichselberger, W., Herdin, M., Ozcelik, H., and Bonek, E., "A Stochastic MIMO Channel Model with Joint Correlation of Both Link Ends," *IEEE Transactions on Wireless Communications*, Vol. 5, No. 1, 2006, pp. 90–100.

[20] Lim, S., Yun, Z., Baker, J., Celik, N., Youn, H., and Iskander, M., "Radio Propagation in Stairwell: Measurement and Simulation Results," *Proceedings of the IEEE International Conference on Wireless Information Technology and Systems*, 28 Aug.–3 Sep. 2010, pp. 1–4.

[21] Yun, Z., Zhang, Z., and Iskander, M. F., "A Ray-Tracing Method Based on the Triangular Grid Approach and Application to Propagation Prediction in Urban Environments," *IEEE Transactions on Antennas and Propagation*, Vol. 50, No. 5, May 2002, pp. 750–758.

[22] Palchak, D., and Farhang-Boroujeny, B., "A Software Defined Radio Testbed for MIMO Systems," *Proceedings of the 2006 Software Defined Radio Technical Conference and Product Exhibition*, 13–17 Nov. 2006.

Ella Atkins
Associate Editor